

NJC

New Journal of Chemistry

A journal for new directions in chemistry

Accepted Manuscript

This article can be cited before page numbers have been issued, to do this please use: G. Zhang, X. Zhao, J. Zou, Y. Shen, M. Lu, Y. Wang, J. Yang and G. Liu, *New J. Chem.*, 2025, DOI: 10.1039/D5NJ02594J.



This is an Accepted Manuscript, which has been through the Royal Society of Chemistry peer review process and has been accepted for publication.

Accepted Manuscripts are published online shortly after acceptance, before technical editing, formatting and proof reading. Using this free service, authors can make their results available to the community, in citable form, before we publish the edited article. We will replace this Accepted Manuscript with the edited and formatted Advance Article as soon as it is available.

You can find more information about Accepted Manuscripts in the [Information for Authors](#).

Please note that technical editing may introduce minor changes to the text and/or graphics, which may alter content. The journal's standard [Terms & Conditions](#) and the [Ethical guidelines](#) still apply. In no event shall the Royal Society of Chemistry be held responsible for any errors or omissions in this Accepted Manuscript or any consequences arising from the use of any information it contains.

Protein-Derived Carbon-Supported Ni-Mo Bimetallic Catalysts with Dual-Active Interfaces for Mild Hydrogenation of Nitroarenes

Guangji Zhang,^{*a} Xiaojun Zhao,^b Jiao Zou,^a Yuqiu Shen,^a Ming Lu,^a Yuhang Wang,^a

Jinyu Yang^{*a} and Guocong Liu^{*a}

^a*School of Chemistry and Materials Engineering, Huizhou University, Huizhou, Guangdong, 516001 P. R. China.*

^b*School of Materials Science and Engineering, Hunan University of Technology, Zhuzhou, Hunan 412007, P. R. China.*

*Corresponding authors: Phone/Fax: +86-0752-2527139

E-mail Addresses: zhanggj1206@hzu.edu.cn (G. Zhang), yangjinyu@hzu.edu.cn (J. Yang) and gcl_109@hzu.edu.cn (G. Liu)

Abstract: Nickel-based non-precious metal hydrogenation catalysts have attracted widespread attention due to their cost-effectiveness, but they still face challenges in practical applications, such as low hydrogenation activity, easy aggregation and deactivation of Ni nanoparticles, and harsh reaction conditions. To address these issues, this study proposes a synergistic strategy based on nitrogen-rich biomass precursors. By leveraging the chelating effect of proteins, NiCl_2 and Na_2MoO_4 were co-assembled on the surface of porous carbon black, followed by pyrolysis under a nitrogen atmosphere, successfully preparing a carbon-supported Ni-MoC bimetallic catalyst with MoC-NiN_x interfaces (Ni-MoC/NC-X). The nitrogen species derived from proteins not only facilitated the formation of a nitrogen-doped carbon (NC) support but also effectively suppressed the aggregation of Ni through N coordination. Furthermore, the synergistic effect between MoC and NiN_x significantly enhanced the activity and stability of the nickel catalyst. Experimental results demonstrated that Ni-MoC/NC700 exhibited high conversion (>99%) and selectivity (>95%) for 16 aromatic nitro compounds with different substituents under mild conditions (90 °C, 5 bar H₂).

Keywords: Synergistic effect; Carbon-supported; Nickel-based catalyst; Heterogeneous catalysis; Nitro hydrogenation

1. Introduction

Aromatic amines are essential intermediates for the synthesis of pharmaceuticals, pesticides, dyes, and advanced polymers, and the development of efficient preparation processes for them has attracted much attention¹. Currently, the catalytic hydrogenation route of aromatic nitro compounds is commonly used in the industry to produce aromatic amino compounds, which has the advantages of high atom economy, low by-products, and environmentally friendly compared with the traditional stoichiometric reduction methods (e.g., Fe/HCl, Na₂S, etc.)². Although noble metal catalysts (e.g., Pt, Pd) exhibit excellent catalytic hydrogenation activity, their prohibitive cost and scarcity limit widespread industrial application³.

In recent years, non-noble catalysts such as Fe, Ni, and Co have attracted widespread attention because of their low cost. However, they still face the problems of harsh reaction conditions (high temperature, high H₂ pressure), poor selectivity, and deactivation due to the leaching or sintering of metal⁴⁻⁸. Among them, carbon-supported nickel-based catalysts have been extensively studied due to their economic viability in preparation. Nevertheless, carbon-supported monometallic nickel catalysts have inherent drawbacks: (i) weak metal-support interaction, leading to Ni leaching during reactions and poor cycling stability⁹; (ii) easy migration and agglomeration of Ni nanoparticles on the carbon carrier surface, resulting in a reduction of active sites¹⁰; and (iii) the intrinsic activity of single Ni active sites remains significantly lower than that of noble metal catalysts¹¹⁻¹³. These shortcomings originate from the inability of the electronic properties at the metal-support interface in nickel-based catalysts to meet the requirements for highly efficient catalysis^{6, 14}.

Modulation of the local chemical environment of active sites is a key strategy to enhance catalytic performance^{15, 16}. Studies have demonstrated that constructing bimetallic catalysts can effectively modulate the d-band electronic structure and enhance the hydrogen spillover effect, thereby improving hydrogenation activity and stability¹⁷⁻¹⁹. By introducing a second metal (e.g., Mo, Cu, or W), the d-band center of Ni can be tuned, the hydrogen spillover effect can be amplified, and catalyst stability can be enhanced^{16, 20-22}. For instance, molybdenum carbide, with its platinum-like d-

band properties, forms a heterostructure with Ni, leading to synergistic catalytic effects in reactions such as CO hydrogenation^{6, 23, 24}. Moreover, support interface engineering plays a critical role. A nitrogen-doped carbon (NC) matrix can anchor metal nanoparticles via strong metal-support interactions (SMSI), preventing aggregation and detachment of Ni active components, thus boosting the catalytic performance of nickel-based catalysts²⁵⁻²⁷. However, current synthetic methods (e.g., those based on metal-organic frameworks (MOFs)) often require complex precursor preparation, which hinders the precise construction and scalable synthesis of bimetallic active sites²⁸⁻³⁰. Based on the above considerations, this study proposes a synergistic strategy using nitrogen-rich biomass precursors: By co-assembling protein, NiCl₂, and Na₂MoO₄ on porous carbon black to form a precursor, followed by pyrolysis under a nitrogen atmosphere, we successfully prepared a nitrogen-doped carbon-supported Ni-MoC bimetallic catalyst (denoted as Ni-MoC/NC-X). This process simultaneously achieves protein carbonization, metal species reduction, and the formation of MoC-NiN_x interfaces. In this catalyst system, the protein serves as both nitrogen and carbon sources, while the carbon black acts as a porous substrate. The chelating effect of the protein enables in-situ anchoring of Ni-Mo bimetallic species. During pyrolysis, the nitrogen species derived from protein decomposition not only facilitate the formation of an NC (nitrogen-doped carbon) matrix on the carbon support but also suppress the agglomeration of Ni nanoparticles through coordination effects. More importantly, the synergistic interaction between MoC and NiN_x enhances the hydrogenation activity of the bimetallic catalyst. Experimental results demonstrate that this catalyst exhibits excellent hydrogenation activity and selectivity for aromatic nitro compounds under mild conditions. Specifically, the Ni-MoC/NC700 catalyst achieves high conversion and selectivity for 16 different substituted aromatic nitro compounds at 90 °C and 5 bar H₂. This work provides a new strategy for the rational design of highly efficient non-noble metal hydrogenation catalysts.

2. Results and Discussion

2.1 Catalyst Characterization

The phase composition of the as-prepared solid samples was initially investigated using XRD. The phase composition was determined by comparing the XRD diffraction patterns of the samples with standard reference patterns. As shown in Fig. 1 and Fig. S1, all catalyst samples exhibit a characteristic peak at 25.2° in their XRD patterns, corresponding to the (002) plane of graphitic carbon. In the molybdenum-containing Ni-MoC/NC-X catalysts, three distinct peaks are observed at 31.83° , 35.75° , and 48.61° , which can be assigned to the (001), (100), and (101) planes of MoC, respectively. Similar peaks are also present in the MoC/NC700 catalyst.

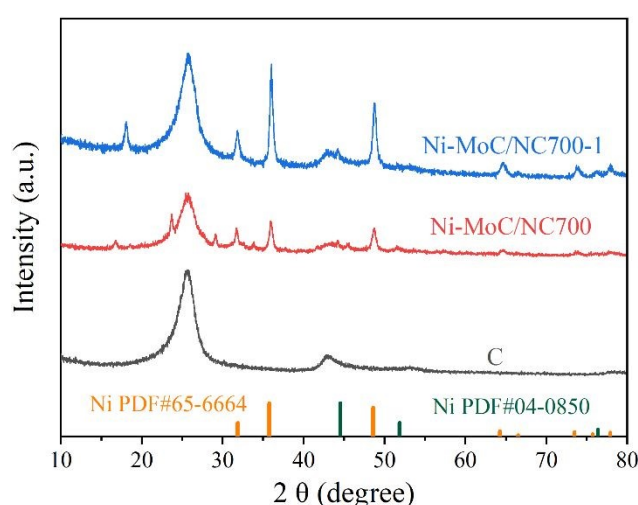


Fig. 1 XRD pattern of Ni-MoC/NC700 catalysts with different Ni loadings.

For the Ni-MoC/NC700-1 sample, where the Ni content increases while Mo content decreases, distinct Ni-related peaks become apparent. Notably, no peaks corresponding to sodium molybdate are detected, indicating complete conversion of the molybdate precursor into MoC during synthesis. In the Ni/NC700-1 sample, three peaks located at 44.5° , 51.84° , and 76.37° are observed, corresponding to the (111), (200), and (220) planes of metallic Ni, respectively. This suggests significant aggregation of Ni species into nanoparticles during the 700°C pyrolysis process. However, when the Ni loading is reduced to one-sixth of that in Ni/NC700-1, no Ni-related peaks are detected in the Ni/NC700 sample, demonstrating that Ni species remain atomically dispersed and effectively anchored on the support without nanoparticle formation. In summary, these results confirm that the Ni species in the Ni-MoC/NC700 catalyst maintain excellent

dispersion without any detectable aggregation.

View Article Online
DOI: 10.1039/D5NJ02594J

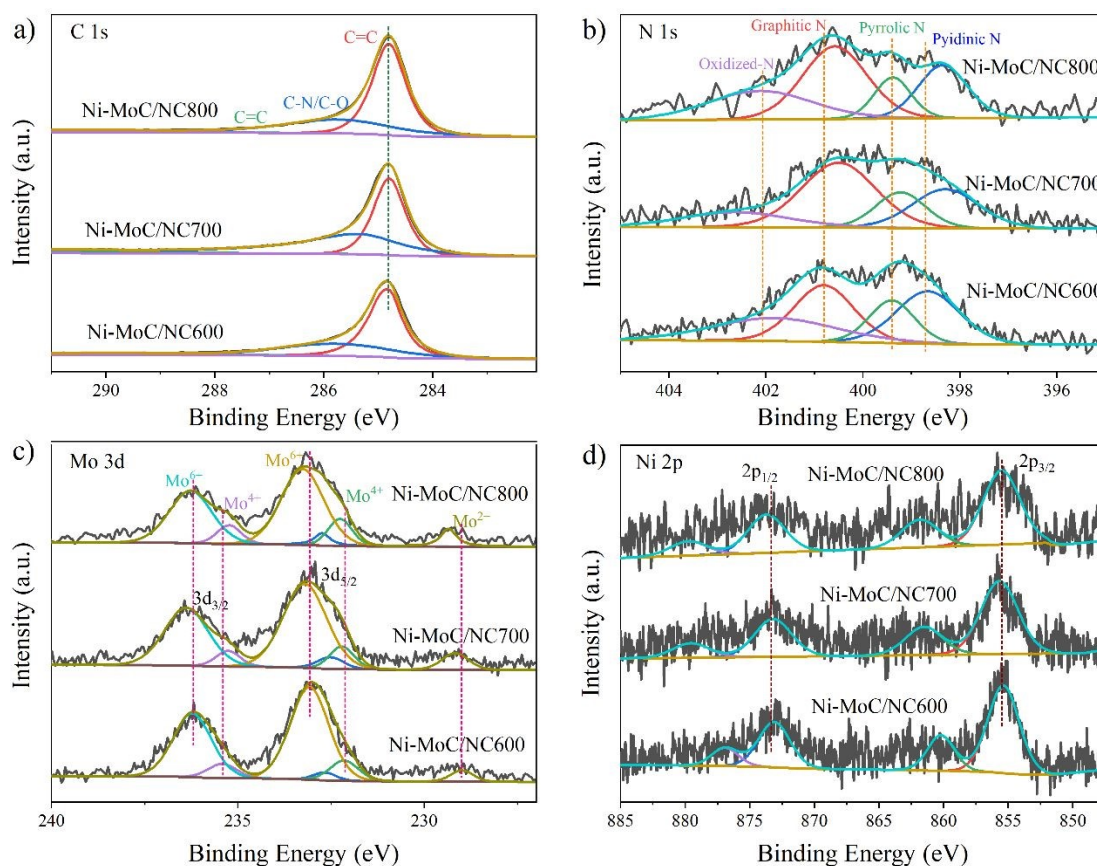


Fig. 2 XPS patterns of Ni-MoC/NC-X, a) C 1s. b) N 1s. c) Mo 3d. d) Ni 2p.

To further determine the chemical composition and structure of the catalyst Ni-MoC/NC-X, high-resolution XPS spectra of the samples were collected and analyzed. The XPS spectra confirmed the presence of Ni, Mo, C, and N in the catalyst sample (as shown in Fig. S2 and Table S2). In the high-resolution Ni 2p spectrum of the Ni-MoC/NC-X sample (Fig. 2d), peaks at 855.67 eV and 873.18 eV correspond to Ni 2p_{3/2} and Ni 2p_{1/2}, respectively^{31, 32}. A slight blue shift in the Ni 2p_{3/2} peak (855.67 eV) indicates the interaction between Ni and other components, such as N. In the high-resolution Mo 3d spectra (Fig. 2c), the peaks at 229.17 and 232.52 eV are attributed to 3d_{5/2} and 3d_{3/2} of Mo²⁺, respectively, indicating the formation of the Mo_xC phase. The peaks at 232.21 and 235.26 eV, attributed to 3d_{5/2} and 3d_{3/2} of Mo⁴⁺, respectively, demonstrate the presence of MoC³³. Additionally, the peaks at 233.20 and 236.38 eV correspond to 3d_{5/2} and 3d_{3/2} of Mo⁶⁺, indicating the partial existence of Mo⁶⁺ on the catalyst surface. The Mo peaks also exhibit a slight blue shift with increasing pyrolysis

temperature, implying that higher temperatures promote interactions between Mo and other components, further supporting the formation of MoC species and their interaction with N and Ni species. The C 1s spectra of the three different Ni-MoC/NC-X catalysts are similar and can be deconvoluted into three peaks (Fig. 2a) located at 284.8 eV, 285.36 eV, and 291.18 eV, which are assigned to C=C, C-O/C=N, and C-O-C/C-N types of carbon, respectively³⁴. In the N 1s spectrum of the Ni-MoC/NC700 catalyst (Fig. 2b), four peaks are observed at 398.30 eV, 399.22 eV, 400.50 eV, and 402.63 eV, corresponding to pyridinic N, pyrrolic N, graphitic N, and oxidized N, respectively^{35, 36}. As shown in Table S3, among the obtained N-doped catalyst materials, graphitic N accounts for the highest proportion and is the predominant nitrogen species. The partial shifts of pyridinic N, pyrrolic N, and graphitic N in the Ni-MoC/NC700 and Ni-MoC/NC800 samples indicate that, as the pyrolysis temperature increases, N interacts with Ni to form NiN_x species.

The defective structure of the carbonaceous surface of the carbon support can be represented by Raman spectroscopy. As shown in Fig. S3, the Raman spectra exhibit two peaks at 1340 cm⁻¹ (D-band) and 1575 cm⁻¹ (G-band), corresponding to the disordered and graphitic nature of the carbon structure, respectively. The intensity ratio (I_D/I_G) reflects the defect density of the carbon matrix. The calculated I_D/I_G values for Ni-MoC/NC600, Ni-MoC/NC700, Ni-MoC/NC800, Ni-NC700, and MoC/NC-700 are 0.82, 0.81, 0.78, 0.91, and 0.88, respectively. The ratio is unchanged after 700 °C pyrolysis of the carbon material surface-coated complexes, indicating that the defect level of the pyrolyzed material does not significantly differ from that of carbon black. Analyzing the pore structure of the Ni-MoC/NC-X catalyst materials through N₂ adsorption/desorption isotherms and pore size distribution. As shown in Table S4, the Ni-MoC/NC-X catalysts exhibit lower adsorption volumes compared to the pure carbon precursor. The specific surface area (S_{BET}) and total volume (V_{total}) are as follows: Ni-MoC/NC600 (49 m²·g⁻¹, 0.171 cm³·g⁻¹) < Ni-MoC/NC700 (64 m²·g⁻¹, 0.240 cm³·g⁻¹) < Ni-MoC/NC800 (79 m²·g⁻¹, 0.306 cm³·g⁻¹) < Acetylene black (106 m²·g⁻¹, 0.332 cm³·g⁻¹). As illustrated in Fig. 3a, the Ni-MoC/NC-X catalysts display similar

adsorption isotherms, with reduced adsorption volumes compared to acetylene black. The lower adsorption capacity at low pressures indicates weak interaction between the catalysts and N_2 . The adsorption isotherms exhibit a Type IV shape, while the presence of a distinct hysteresis loop at high pressures suggests the existence of macropores in the samples. Additionally, the hysteresis loop observed in the relative pressure (P/P_0) range of 0.5~0.8 indicates the presence of mesopores in the materials. As shown in Fig. 3b, the pore size distribution of the samples was investigated to study their pore structure. The Ni-MoC/NC-X samples possess a hierarchical pore structure, with a small number of micropores primarily distributed in the 1~2 nm range, mesopores mainly distributed in the 2~40 nm range, and macropores predominantly located in the 76~79 nm range. To further validate the results, we employed the Horvath-Kawazoe (H-K) method and successfully confirmed the presence of micropores (Fig. S4). The hysteresis loop in Fig. 3a is not prominent, which may be attributed to the micro-meso-macroporous structure of the material, with mesopores partially obstructed. Among them, the Ni-MoC/NC700 catalyst exhibits a higher proportion of micropores compared to Ni-MoC/NC600 and Ni-MoC/NC800. Therefore, this hierarchical pore characteristic of the Ni-MoC/NC700 catalyst contributes to enhanced catalytic hydrogenation performance.

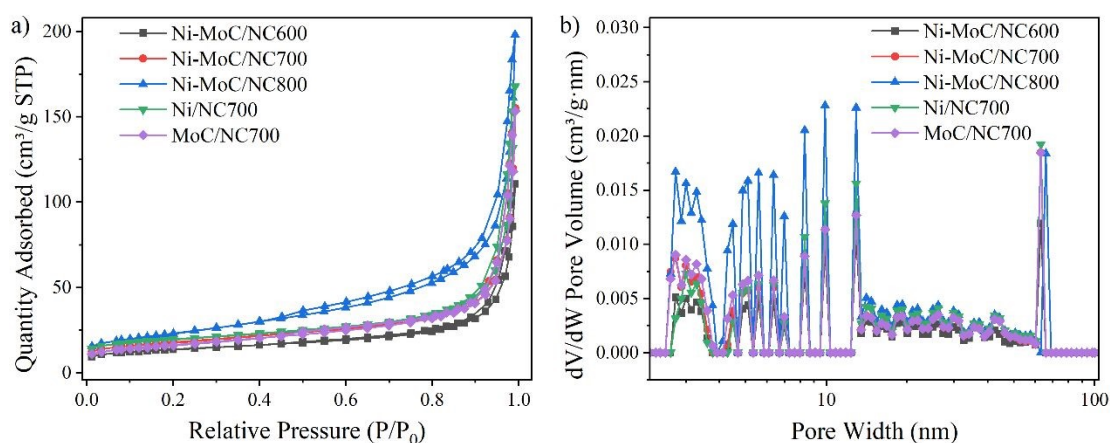


Fig. 3 a) N_2 adsorption/desorption isotherm and b) pore size distribution of Ni-MoC/NC-X.

To investigate the morphological structure of the Ni-MoC/NC-X catalysts, we performed SEM and TEM analyses on the samples. As shown in Fig. 4 and Fig. S5,

after carbonization, the composites exhibited minimal morphological changes compared to acetylene black. The samples displayed similar morphologies, all consisting of stacked spherical structures with a relatively uniform size distribution. This indicates that during the synthesis process, the catalysts prepared with acetylene black retained the morphological structure of acetylene black, whereas the catalysts carbonized directly from the nickel-molybdenum protein precursor formed bulk carbon matrices.

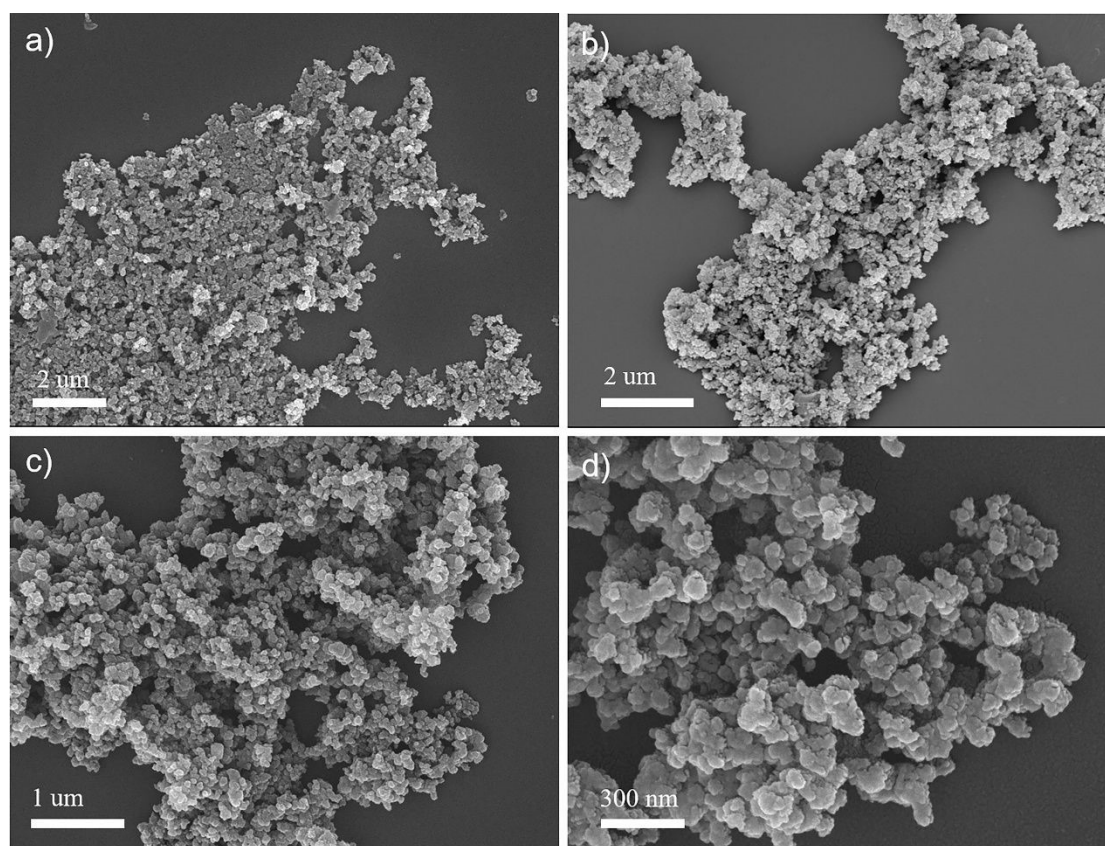


Fig. 4 SEM images of the Ni-MoC/NC700 catalyst at different magnifications.

The morphology of the catalysts was further characterized by TEM. As shown in Fig. 5 and Fig. S6, the catalyst samples Ni-MoC/NC700, Ni-MoC/NC600, and MoC/NC700 exhibited similar morphological features. The flake-like structures in the images represent the carbon substrate, with MoC particles dispersed on the surface of the flakes. HR-TEM analysis at high resolution revealed that all catalysts had thin layers of MoC locally distributed on the carbon support surface, with lattice fringes distinct from those of the carbon matrix, with a measured interplanar spacing of 0.19 nm, which matches

the (100) crystal plane of MoC. High-angle annular dark-field scanning transmission electron microscopy (HAADF-STEM) and corresponding energy-dispersive X-ray spectroscopy (EDS) elemental mapping of the Ni-MoC/NC700 catalyst demonstrate the uniform distribution of nickel (Ni), molybdenum (Mo), carbon (C), and nitrogen (N) on the carbon support. These results indicate the occurrence of metal-support interaction during catalyst synthesis, particularly in samples doped with N and Mo.

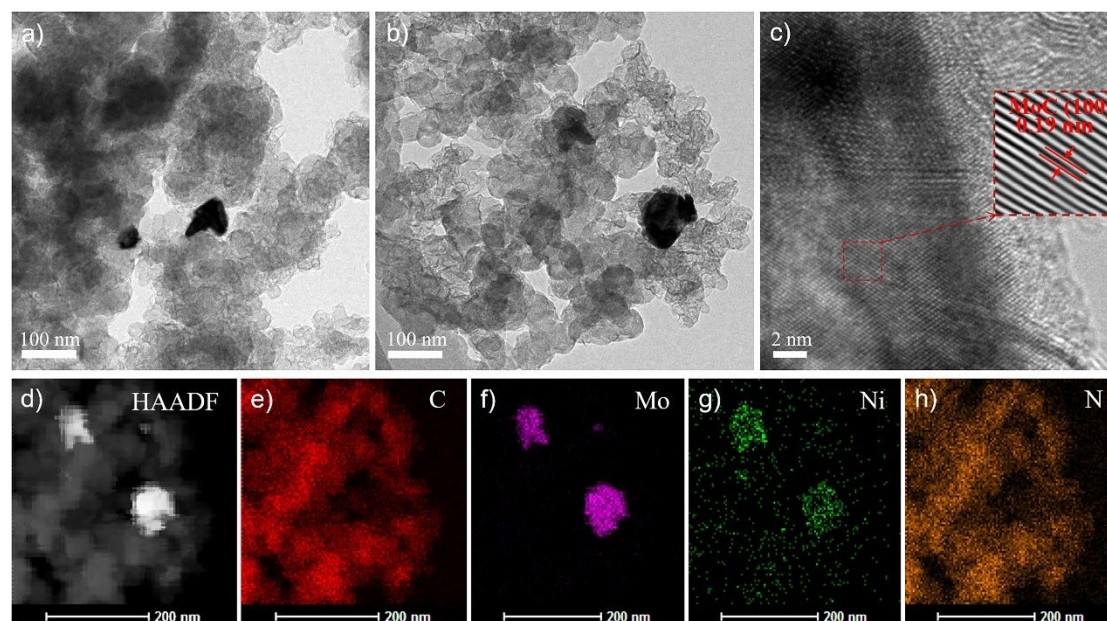


Fig. 5 TEM images of a,b) Ni-MoC/NC700. c) local HRTEM image, d) HAADF-STEM image, and e-h) corresponding EDS element mapping of Ni-MoC/NC700.

To investigate the hydrogen adsorption capacity of the catalysts, we performed H_2 programmed temperature desorption (H_2 -TPD) experiments. As shown in Fig. 6, the H_2 -TPD profiles of Ni-MoC/NC700, MoC/NC700, and Ni/NC700 exhibit two distinct desorption peaks. Among the catalysts, those containing MoC species exhibit a significantly higher hydrogen desorption capacity (Table S5), indicating that MoC serves as the primary active site for hydrogen adsorption and activation. Generally, the low-temperature desorption peak arises from the desorption of chemically adsorbed H from active sites, while the high-temperature peak is associated with the spillover of H species. For Ni-MoC/NC700, the low-temperature desorption peak appears at 170 °C, similar to Ni/NC700 (169 °C). In contrast, MoC/NC700 shows a higher desorption temperature (243 °C). Mass spectrometry (MS) analysis (Fig. S7) confirmed that this

peak in MoC/NC700 does not originate from hydrogen desorption, suggesting it may arise from other adsorbed species. Regarding the high-temperature desorption peak, Ni-MoC/NC700 exhibits a significantly lower hydrogen spillover temperature (474 °C) compared to Ni/NC700 (505 °C) and MoC/NC700 (485 °C), indicating that dissociated hydrogen species desorb more readily from the Ni-MoC/NC700 catalyst. Therefore, the incorporation of MoC facilitates H₂ activation on the Ni-based catalyst. Overall, the H₂-TPD results indicated that the interaction between MoC and Ni sites on the carbon support promotes H₂ activation, thereby enhancing the hydrogenation activity of the catalyst.

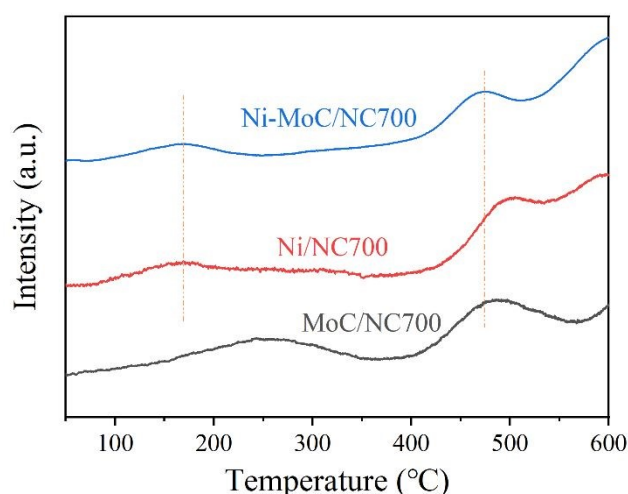


Fig. 6 H₂-TPD profiles of Ni-MoC/NC700, MoC/NC700, and Ni/NC700 catalysts.

To verify the existence of dual active sites on the Ni-MoC/NC700 catalyst interface, we conducted NH₃-TPD and CO₂-TPD characterizations to demonstrate the presence of dual catalytic active sites in the bimetallic catalyst. NH₃-TPD was used to characterize the acidic sites and acid quantities of the catalyst. For different acidic sites, the adsorbed substances generally desorb at distinct temperatures. Typically, the stronger the acidity of an adsorption site, the greater the adsorption affinity for NH₃, and the higher the temperature required for desorption. As shown in Fig. 7a and Table S6, the NH₃-TPD profile of Ni-MoC/NC700 exhibits three distinct desorption peaks for Ni-MoC/NC700 at 140.8 °C (weak acid sites), 392.9 °C (medium acid sites), and 486.2 °C (strong acid sites, acid quantity of 360.5 μmol g⁻¹). In contrast, the

MoC/NC700 only showed weak (95.7 °C) and medium (386.1 °C) acid sites without significant high-temperature peaks (>400 °C). Similarly, CO₂-TPD characterization confirmed the presence of basic sites in the catalyst. As shown in Fig. 7b, both Ni-MoC/NC700 and Ni/NC700 catalysts exhibit desorption peaks across three temperature regions (weak basic sites: <200 °C; medium-strong basic sites: 200–400 °C; strong basic sites: >400 °C), with overlapping peaks observed in the medium-high temperature range. For Ni-MoC/NC700, the three desorption peaks at 86.6 °C, 393.5 °C, and 548.6 °C correspond to weak, medium, and strong basic sites, respectively, with a total basic site content of 50.7 μmol g⁻¹ (Table S7). In comparison, Ni/NC700 exhibits the highest basic site content (111.1 μmol g⁻¹) in the medium basic site region, though its total basic site content (206.2 μmol g⁻¹) is significantly higher than that of Ni-MoC/NC700. This suggests that increased Ni doping provides more basic sites, primarily attributed to NiN_x species³⁷, while Mo species contribute acidic sites^{38, 39}. The combined NH₃-TPD and CO₂-TPD results confirm that the Ni-MoC/NC700 catalyst possesses dual active sites (acidic and basic sites), which synergistically enhance its hydrogenation catalytic activity.

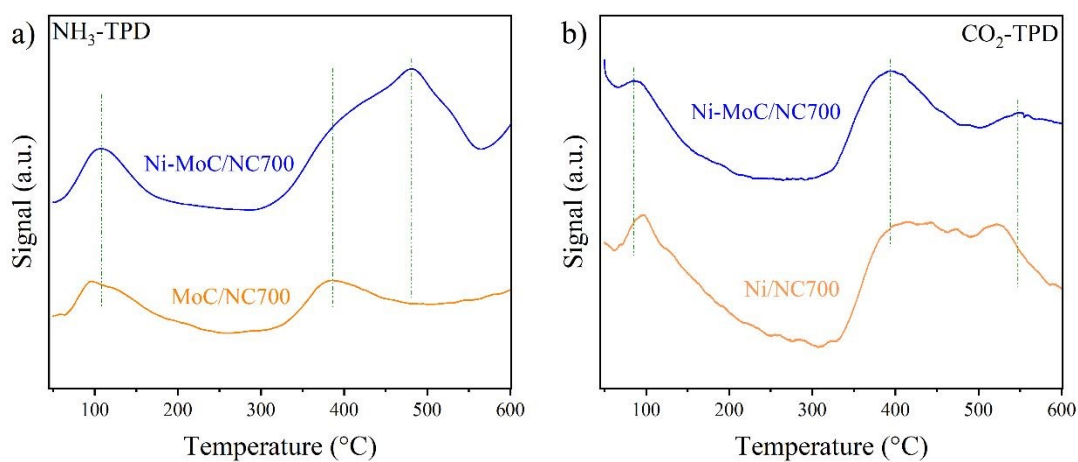


Fig. 7 a) NH₃-TPD, and b) CO₂-TPD profiles of the different catalysts.

2.2 Catalyst Performance Testing

The hydrogenation performance of the prepared catalysts for nitro compounds was evaluated. As shown in Table 1, the catalysts Ni-MoC/C700 and MoC/NC700 showed very low conversion rates (≈4%) for p-chloronitrobenzene, indicating that nickel metal

sites are the primary high-activity centers for hydrogenation in these catalysts. Nitrogen doping facilitates the formation of NiN_x species, significantly enhancing the catalytic hydrogenation activity. The MoC/NC700-Ni catalyst, prepared via stepwise loading, also exhibited relatively low activity (*Con.*: 9.5%), with no significant improvement observed. The conversion rates of p-chloronitrobenzene over Ni/NC700 and Ni/NC700–1 were 27.1% and 18.5%, respectively, suggesting that higher nickel loading does not improve the catalytic performance of Ni-based catalysts. Instead, excessive nickel loading leads to particle agglomeration, reducing activity. The catalysts Ni-MoC/NC600, Ni-MoC/NC700, and Ni-MoC/NC800 achieved conversion rates of 17.5%, 99.9%, and 96.8%, respectively, with \approx 99% selectivity for p-chloronitrobenzene. In contrast, Ni-MoC/NC700–1 showed a conversion rate of only 58.7%, indicating that a substantial increase in nickel loading decreases activity. When the protein content was further increased to prepare Ni-MoC/NC700–2, the conversion rate dropped to 42.1%. This decline is attributed to excessive protein carbonization, which forms a thick carbon layer that encapsulates nickel active sites, reducing their availability. Under optimized conditions, the Ni-MoC/NC700 catalyst can also carry out the catalytic hydrogenation of p-chloronitrobenzene under mild conditions (25 °C and 5 bar).

Table 1. Catalytic hydrogenation of p-chloronitrobenzene over various catalysts.

Entry	Catalyst	<i>T</i> (°C)	<i>P</i> (bar)	<i>Con.</i> (%)	<i>Sel.</i> (%)
1	Ni-MoC/NC600	90	5	17.5	98.9
2	Ni-MoC/NC700	90	5	99.9	99.9
3	Ni-MoC/NC800	90	5	96.8	99.8
4	Ni-MoC/NC700–1	90	5	58.7	99.1
6	Ni/NC700–1	90	5	18.5	99.9
7	Ni/NC700	90	5	27.1	99.3
8	MoC/NC700-Ni	90	5	9.5	99.9
9	MoC/NC700	90	5	4.1	99.9
10	Ni-MoC/NC700–2	90	5	42.1	99.8
11	Ni-MoC/C700	90	5	3.8	90.5

12^a Ni-MoC/NC700 25 5 22.3 86.4

View Article Online
DOI: 10.1039/D5NJ02594J

Reaction conditions: 0.25 mmol of p-chloronitrobenzene with 50 mg catalyst in 5 mL H₂O at 90 °C and 5 bar H₂ pressure for 5 h. ^a48h.

In summary, the optimal catalyst was determined to be Ni-MoC/NC700, which achieved 99.9% conversion of p-chloronitrobenzene with 99.9% selectivity under the reaction conditions of 90 °C, 5 bar H₂ pressure for 5 h. Remarkably, this catalyst could also catalyze the hydrogenation reduction of p-chloronitrobenzene at room temperature. The superior catalytic performance of Ni-MoC/NC700 can be attributed to the synergistic effects between its hierarchical pore structure and the bimetallic active sites (NiN_x and MoC). Notably, Ni-MoC/NC700 is one of the outstanding catalysts for nitroarene hydrogenation reactions, with a turnover frequency (TOF) value of 8.1 h⁻¹. Although this value is lower than that of some other state-of-the-art catalysts, such as NiMo₂C/SBA-15 (11.9 h⁻¹), Co-phthalocyanine (Co-Pc, 9.6 h⁻¹), and Co-100-NAC (14.1 h⁻¹), it outperforms most recently reported Ni-based catalysts in terms of catalytic performance (Table S8).

Table 2. Catalytic hydrogenation of p-chloronitrobenzene in various solvents.

Entry	Catalyst	Solvent	<i>T</i> (°C)	<i>Con.</i> (%)	<i>Sel.</i> (%)
1	Ni-MoC/NC700	H ₂ O	90	100	99.9
2	Ni-MoC/NC700	EtOH/H ₂ O	90	100	99.9
3	Ni-MoC/NC700	MeOH	90	84.5	98.7
4	Ni-MoC/NC700	EtOH	90	51.8	99.9
5	Ni-MoC/NC700	IPA	90	52.2	99.9
6	Ni-MoC/NC700	MeCN	90	24	96.0
7	Ni-MoC/NC700	DMF	90	27.1	89.0
8	Ni-MoC/NC700	Hexane	90	31.2	99.9

Reaction conditions: 0.25 mmol of p-chloronitrobenzene, Catalysts 50 mg, 5 ml of solvents, 90 °C, 5 h and 5 bar of H₂. Conversion (C) of reactant and selectivity (S) were determined by HPLC.

The influence of different solvents on catalytic performance was subsequently

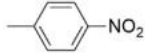
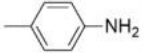
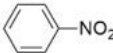
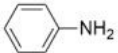
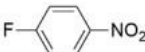
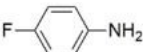
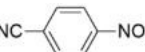
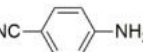
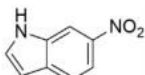
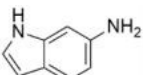

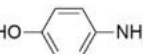

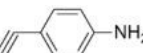
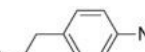
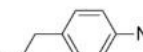
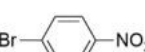
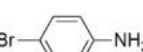
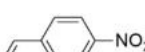
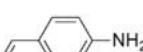
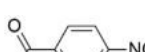
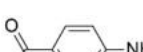




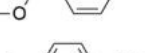
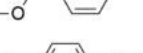

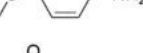
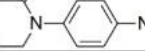
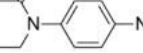
investigated. As shown in Table 2, relatively low conversion rates of p-chloronitrobenzene were observed in aprotic solvents: n-Hexane (31.2%), DMF (27.1%), and MeCN (24%). In contrast, higher conversions were achieved in protic solvents: EtOH (51.8%), MeOH (84.5%), and IPA (isopropanol, 52.2%). Particularly, the presence of H₂O significantly promoted the nitro hydrogenation reaction, yielding complete conversion (100%). Therefore, it can be concluded that protic solvents, including H₂O, EtOH, MeOH, IPA, and EtOH/H₂O, effectively enhance the nitro hydrogenation performance of the Ni-MoC/NC700 catalyst.

The kinetic study of p-chloronitrobenzene hydrogenation reduction over the Ni-MoC/NC700 catalyst was investigated. As shown in Fig. S8, the conversion of p-chloronitrobenzene progressively increased with reaction time, gradually converting to 4-chloroaniline. During the catalytic process, only 4-hydroxylaminobenzene was detected as an intermediate product, while no other intermediates, such as azo compounds were detected (Fig. S9).

In summary, Ni-MoC/NC700 demonstrated superior catalytic performance as the optimal catalyst. To verify its universality in the hydrogenation reduction of nitro compounds, substrate scope expansion was conducted with results shown in Table 3. The data reveal that Ni-MoC/NC700 exhibits high conversion (>99%) and selectivity (>98%) for all 16 nitro compounds, including alkyl-chain compounds, halogenated compounds, heterocyclic compounds, and unsaturated-group-containing compounds. Firstly, the conversion of alkyl, hydroxyl, aliphatic, ether, and thioether nitro compounds to conventional substrates (substrates 1, 2, 6, 7, 12-15) is more than 99% with a selectivity of >99.0%. Similarly, for halogenated nitro compounds, the conversion was >99% and the selectivity was >98%, with virtually no dehalogenation occurring (substrates 3, 9). In addition to this, high selectivity (*Con.*: >99%, *Sel.*: 93.5%-99.9%) was achieved for nitro compounds containing unsaturated groups (substrates 4, 7, 10, and 16) such as aldehydes, nitriles, alkynes, and alkenes. Finally, the catalysts also exhibited high catalytic performance (*Con.*: >99%, *Sel.*: 97-99.9%) for heterocyclic nitro compounds (substrates 5 and 15). In conclusion, the catalyst Ni-MoC/NC700 demonstrates exceptional catalytic activity for nitro compound

hydrogenation under mild conditions (5 bar, 90 °C), owing to the synergistic interplay between its hierarchical pore structure and the dual active sites (NiN_x and MoC).

Table 3. Catalytic hydrogenation of nitroarenes over the Ni-MoC/NC700 catalyst.

Entry	Substrates	Products	Con. (%)	Sel. (%)
1			>99	99.1
2			>99	99.9
3			>99	99.5
4			>99	99.9
5			>99	97.0
6			>99	99.9
7			>99	95.2
8			>99	99.9
9			>99	98.1
10			>99	93.5
11			>99	99.9
12			>99	99.9
13			>99	99.9
14			>99	99.6
15			>99	99.9
16			>99	99.9

Reaction conditions: 0.25 mmol substrate, 50 mg catalyst, 5 ml EtOH/H₂O, 90 °C, 5 bar H₂, 5 h.

The recycling stability of Ni-MoC/NC700 was finally evaluated. Under low conversion conditions, the catalytic performance slightly decreased after the first cycle,

but the hydrogenation performance stabilized in subsequent cycles (Fig. 8), maintaining a conversion rate of approximately 40%. Under high conversion conditions (Fig. S10), the catalyst retained high catalytic activity even after 5 cycles (*Con.*: 97.5%, *Sel.*: 99.8%). XRD analysis of the recycled catalyst revealed no phase change in the MoC component, while SEM characterization showed preserved porosity and structural integrity (Fig. S11). Subsequently, ICP-OES analysis was performed to measure the Ni and Mo contents in the Ni-MoC/NC700 catalyst before and after the reaction. The optimal Ni-MoC/NC700 catalyst contained 0.65 wt.% Ni and 2.6 wt.% Mo, while the recovered catalyst exhibited minor changes in metal content (Table S9). These results further confirm the stability of Ni-MoC/NC700 during the hydrogenation reaction process.

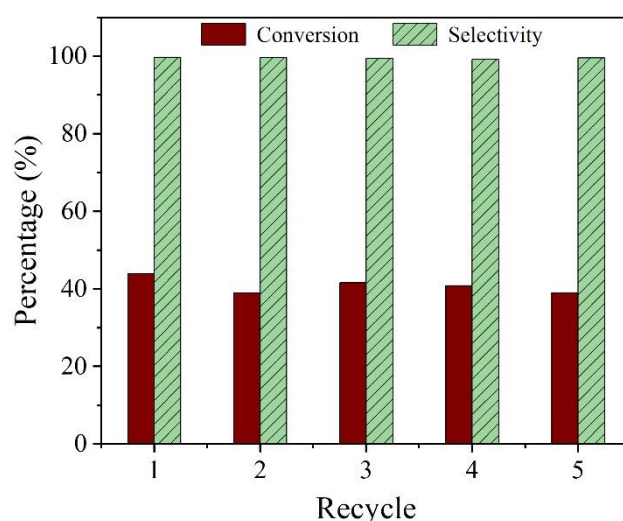


Fig. 8 Recycling of the Ni-MoC/NC700 catalyst. Reaction conditions: 100 mg catalyst, 0.25 mmol p-chloronitrobenzene, 10 mL H₂O, 90 °C, 5 bar H₂, 1.5 h.

3. Conclusion

In summary, we successfully developed N-doped porous carbon-supported nickel-molybdenum bimetallic catalysts (Ni-MoC/NC-X) through a facile synthesis route involving the complexation of protein, nickel chloride, sodium molybdate, and carbon black, followed by pyrolysis under N₂ atmosphere. The as-prepared catalysts feature a hierarchical pore structure and well-dispersed Ni active sites, where nitrogen doping effectively anchors nickel species and prevents their aggregation, thereby endowing the

catalysts with exceptional hydrogenation performance. Remarkably, the optimized Ni-MoC/NC700 catalyst demonstrates outstanding catalytic activity under mild conditions (90 °C, 5 bar H₂), achieving high conversion and selectivity for a broad range of nitro compounds (16 substrates). Notably, it can even hydrogenate p-chloronitrobenzene under extremely mild conditions (25 °C, 5 bar H₂). The catalyst exhibits excellent stability with negligible activity loss after multiple reaction cycles. Overall, we have developed an N-doped porous carbon-supported nickel-molybdenum bimetallic catalyst (Ni-MoC/NC700) for achieving highly efficient and selective catalytic hydrogenation reduction of aromatic nitro compounds under mild reaction conditions. The outstanding performance of this catalyst can be attributed to the synergistic catalytic effects between NiN_x and MoC active sites. Utilizing cost-effective acetylene black as the support significantly reduces production costs, making this catalyst a promising candidate for industrial-scale catalytic hydrogenation of nitro compounds.

Author Contributions

Guangji Zhang: writing – original draft and data curation; Xiaojun Zhao: visualization and investigation; Jiao Zou: data curation; Yuqiu Shen: investigation; Ming Lu: supervision; Yuhan Wang: investigation; Jinyu Yang: validation and investigation; Guocong Liu: formal analysis, supervision, and methodology. All authors have given approval to the final version of the manuscript.

Data availability

Data will be made available on request.

Conflicts of interest

There are no conflicts of interest to declare.

Acknowledgments

This work was supported by the Professorial and Doctoral Scientific Research Foundation of Huizhou University (No.2022JB056, and 2020JB007), the Key Research

Projects in Colleges and Universities in Guangdong Province (No. 2023ZDZX3036),
and the Guangdong Provincial Key Construction Discipline Research Capability
Enhancement Project (No. 2021ZX089).

References

1. S. Gutiérrez-Tarriño, S. Rojas-Buzo, C. W. Lopes, G. Agostini, J. J. Calvino, A. Corma and P. Oña-Burgos, *Green Chem.*, 2021, **23**, 4490-4501.
2. D. Yadav and S. K. Awasthi, *Green Chem.*, 2020, **22**, 4295-4303.
3. J. Chen, H. Wang, Z. Wang, S. Mao, J. Yu, Y. Wang and Y. Wang, *ACS Catal.*, 2019, **9**, 5302-5307.
4. S. Ibraheem, G. Yasin, A. Kumar, M. A. Mushtaq, S. Ibrahim, R. Iqbal, M. Tabish, S. Ali and A. Saad, *Appl. Catal., B*, 2022, **304**, 120987.
5. R. V. Jagadeesh, A.-E. Surkus, H. Junge, M.-M. Pohl, J. Radnik, J. Rabeah, H. Huan, V. Schünemann, A. Brückner and M. Beller, *Science*, 2013, **342**, 1073.
6. K. Liu, Y. Cao, S. Yang, C. Wu, Z. Zhang, Q. Zhang and H. Zhang, *Ind. Eng. Chem. Res.*, 2020, **59**, 14267-14277.
7. J. R. Morse, J. F. Callejas, A. J. Darling and R. E. Schaak, *Chem. Commun.*, 2017, **53**, 4807-4810.
8. J. P. Southouse, L. Lazzarini, A. O. Ibadon and M. G. Francesconi, *New J. Chem.*, 2021, **45**, 17808-17815.
9. Y. Sun, X. Li, Z. Cai, H. Bai, G. Tang and Z. Hou, *Catal. Sci. Technol.*, 2018, **8**, 4858-4863.
10. T.-S. Kim, J. Kim, H. C. Song, D. Kim, B. Jeong, J. Lee, J. W. Shin, R. Ryoo and J. Y. Park, *ACS Catal.*, 2020, **10**, 10459-10467.
11. Q. Tang, Z. Yuan, S. Jin, K. Yao, H. Yang, Q. Chi and B. Liu, *React. Chem. Eng.*, 2020, **5**, 58-65.
12. Y. Ren, H. Wei, G. Yin, L. Zhang, A. Wang and T. Zhang, *Chem. Commun.*,

- 2017, **53**, 1969-1972.
13. P. Zhang, Z. Zhao, B. Dyatkin, C. Liu and J. Qiu, *Green Chem.*, 2016, **18**, 3594-3599.
14. G. Hahn, J.-K. Ewert, C. Denner, D. Tilgner and R. Kempe, *ChemCatChem*, 2016, **8**, 2461-2465.
15. T. Wang, R. Jin, X. Wu, J. Zheng, X. Li and K. Ostrikov, *J. Mater. Chem. A*, 2018, **6**, 9228-9235.
16. D. Wang, X. Kang, Y. Gu, H. Zhang, J. Liu, A. Wu, H. Yan, C. Tian and H. Fu, *ACS Catal.*, 2020, DOI: 10.1021/acscatal.0c01159, 10449-10458.
17. W. Liu, Y. Yang, L. Chen, E. Xu, J. Xu, S. Hong, X. Zhang and M. Wei, *Appl. Catal., B*, 2020, **282**, 119569.
18. H. Wang, H. Xin, C. Cai, C. Zhu, Z. Xiu, Q. Liu, Y. Weng, C. Wang, X. Zhang, S. Liu, Z. Peng and L. Ma, *ACS Catal.*, 2020, **10**, 10646-10660.
19. S. Jiang, R. Shu, A. Wang, Z. Deng, Y. Xiao, J. Li, Q. Meng and Q. Zhang, *Green Chem.*, 2024, DOI: 10.1039/D4GC02298J.
20. A. Zeng, B. Xu, C. Lu, Y.-Y. Liu, Z. Sun, A. Wang and Y. Wang, *Chem. Eng. J.*, 2024, **500**, 156935.
21. H. Huang, X. Wang, X. Li, C. Chen, X. Zou, W. Ding and X. Lu, *Green Chem.*, 2017, **19**, 809-815.
22. Y. Deng, Y. Ge, M. Xu, Q. Yu, D. Xiao, S. Yao and D. Ma, *Acc. Chem. Res.*, 2019, **52**, 7772-3383.
23. Z. Cao, X. Zhang, R. Guo, S. Ding, P. Zheng, J. Fan, J. Mei, C. Xu and A. Duan, *Chem. Eng. J.*, 2020, **400**, 125886.
24. J. Yu, Y. Yang, L. Chen, Z. Li, W. Liu, E. Xu, Y. Zhang, S. Hong, X. Zhang and M. Wei, *Appl. Catal., B*, 2020, **277**, 119273.
25. Y. Gu, B. Xi, R. Wei, Q. Fu, Y. Qain and S. Xiong, *Nano Lett.*, 2020, **20**, 8375-8383.
26. F. Yang, M. Wang, W. Liu, B. Yang, Y. Wang, J. Luo, Y. Tang, L. Hou, Y. Li, Z. Li, B. Zhang, W. Yang and Y. Li, *Green Chem.*, 2019, **21**, 704-711.
27. J. H. Advani, K. Ravi, D. R. Naikwadi, H. C. Bajaj, M. B. Gawande and A. V.

- Biradar, *Dalton Trans.*, 2020, **49**, 10431-10440.
28. H. Yang, S. J. Bradley, A. Chan, G. I. N. Waterhouse, T. Nann, P. E. Kruger and S. G. Telfer, *J. Am. Chem. Soc.*, 2016, **138**, 11872-11881.
29. J. Li, B. Wang, Y. Qin, Q. Tao and L. Chen, *Catal. Sci. Technol.*, 2019, **9**, 3726-3734.
30. X. Yan, L. Chen, H. Song, Z. Gao, H. Wei, W. Ren and W. Wang, *New J. Chem.*, 2021, **45**, 18268-18276.
31. L. Ning, S. Liao, H. Li, R. Tong, C. Dong, M. Zhang, W. Gu and X. Liu, *Carbon*, 2019, **154**, 48-57.
32. H. Huang, X. Wang, Y. Sheng, C. Chen, X. Zou, X. Shang and X. Lu, *RSC Adv.*, 2018, **8**, 8898-8909.
33. T. Zhang, X. Guo and Z. Zhao, *ACS Appl. Nano Mater.*, 2018, **1**, 3579-3589.
34. V. Goyal, N. Sarki, B. Singh, A. Ray, M. Poddar, A. Bordoloi, A. Narani and K. Natte, *ACS Appl. Nano Mater.*, 2020, **3**, 11070-11079.
35. Q. Luo, C. Wang, H. Xin, Y. Qi, Y. Zhao, J. Sun and F. Ma, *ACS Sustain. Chem. Eng.*, 2021, **9**, 732-742.
36. B. Li, Y. Wang, Q. Chi, Z. Yuan, B. Liu and Z. Zhang, *New J. Chem.*, 2021, **45**, 4464-4471.
37. P. Hou, X. Wang, Z. Wang and P. Kang, *ACS Appl. Mater. Inter.*, 2018, **10**, 38024-38031.
38. J. Li, C. Zhang, Y. Liu, B. Fang, J. Ni, J. Lin, B. Lin and L. Jiang, *AIChE J.*, 2023, **69**, e18194.
39. R. Sakdee, S. Ratchahat, C. Sakdaronnarong, W. Koo-amornpattana, W. Limphirat, S. Mahakot, S. Assabumrungrat and A. Srifa, *Fuel Process. Technol.*, 2025, **276**, 108276.

The data that support the findings of this study are available in this published article and its supplementary information files. The raw datasets generated during and/or analyzed during the current study are available from the corresponding author on reasonable request.

View Article Online
DOI: 10.1039/D5NJ02594J